High Temperature Creep Behavior of Phosphoric Acid-Polybenzimidazole Gel Membranes

Xiaoming Chen,[1] Guoqing Qian,[2] Max A. Molleo,[2] Brian C. Benicewicz,[2] Harry J. Ploehn[1]

[1]Department of Chemical Engineering, University of South Carolina, Columbia, South Carolina 29208
[2]Department of Chemistry & Biochemistry, University of South Carolina, Columbia, South Carolina 29208
Correspondence to: H. J. Ploehn (E-mail: ploehn@cec.sc.edu)

Received 30 April 2015; accepted 13 July 2015; published online 6 August 2015
DOI: 10.1002/polb.23791

ABSTRACT: This work investigates the effects of polymer solids content and macromolecular structure on the high temperature creep behavior of polybenzimidazole (PBI) gel membranes imbibed with phosphoric acid (PA) after preparation via a polyphosphoric acid (PPA) mediated sol-gel process Low-solids, highly acid-doped PBI membranes demonstrate outstanding fuel cell performance under anhydrous, ambient pressure, and high temperature (120–200 °C) operating conditions. However, PBI membranes are susceptible to creep under compressive loads at elevated temperatures, so their long-term mechanical durability is a major concern. Here, we report results for the creep behavior of PBI membranes subject to compression at 180 °C. For para- and meta-PBI homopolymers, increasing polymer solids content results in lower creep compliance and higher extensional viscosity, which may be rationalized by increasing chain density in the sol-gel network. Comparing various homo- and copolymers at similar solids loading, differences in creep behavior may be rationalized in terms of chain–chain and chain-solvent interactions that control macromolecular solubility and stiffness in the PA solvent. The results demonstrate the feasibility of improving the mechanical properties of PA-doped PBI membranes by control of polymer solids content and rational design of PBI macromolecular structure. © 2015 Wiley Periodicals, Inc. J. Polym. Sci., Part B: Polym. Phys. **2015**, *53*, 1527–1538

KEYWORDS: compliance; compression; creep; membranes; polybenzimidazole; polymer electrolyte

INTRODUCTION High temperature polymer electrolyte membranes (PEM) that operate above 120 °C offer many benefits for fuel cell operations, including better tolerance of fuel impurities, improved electrode kinetics, higher ionic conductivities, and reduced requirements for heat and water management. Polybenzimidazole (PBI) polymers doped with phosphoric acid (PA) are promising candidate materials for high temperature PEM fuel cells (PEMFCs). PBI membranes have been utilized in PEMFCs operated for extended periods of time (up to 20,000 h) at temperatures up to 200 °C under anhydrous and ambient pressure conditions.[1–9]

PA-doped PBI membranes are made in two ways: the conventional imbibing method[1] and a recently invented PPA sol-gel process.[9] The conventional imbibing method involves many steps, including condensation polymerization, isolation of polymer, polymer dissolution, membrane casting, solvent removal, film washing and drying, and PA doping. In contrast, the PPA sol-gel process requires only three processing steps. First, appropriate monomers (Fig. 1) are dissolved in polyphosphoric acid (PPA) and polymerized to form PBI polymers. The PPA solution of PBI is then directly cast as a liquid film onto a flat surface. Finally, placing the liquid film in a humid environment results in absorption of water that reacts with PPA to form PA. Because PA is a poor solvent for PBI, the polymer undergoes a sol-gel transition to form a physically cross-linked gel network imbibed with PA. PA-doped PBI membranes made this way are called "sol-gel" membranes. The reduced number of process steps and ease of material handling make the PPA sol-gel process attractive for commercial membrane production.

In fact, PBI sol-gel membranes are Flory type III physical gels[10] that have different structure and physical properties than conventionally imbibed PBI membranes. The latter have acid doping levels (i.e., molar ratio of PA to PBI repeat unit) typically around 5–6, while PBI membranes made by the PPA sol-gel process can achieve acid doping levels greater than 30. Due to their high acid doping levels, PBI sol-gel membranes made by the PPA process exhibit fuel cell performance superior to that of conventionally imbibed membranes.[11–13]

Additional Supporting Information may be found in the online version of this article.

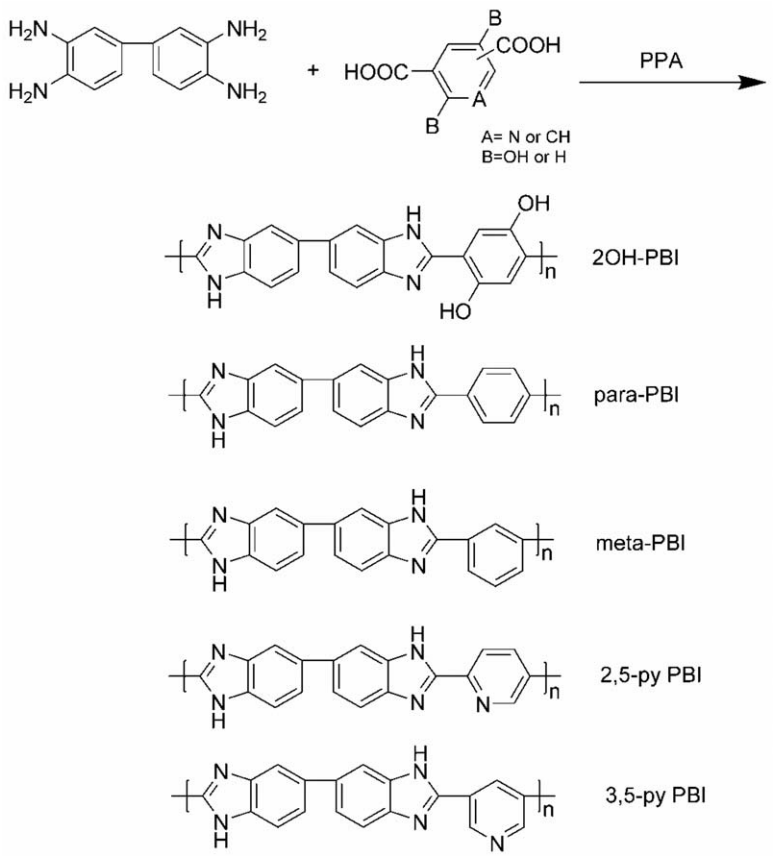

FIGURE 1 Polymerization process for producing different PBI homopolymers, illustrating the chemical structures produced from a variety of monomers.

Successful commercialization of PEMFCs for some applications requires operation for >40,000 h under steady-state conditions or > 5,000 h under dynamic conditions with minimal performance degradation.[14,15] To meet such requirements, a PEM must have not only stable electrochemical properties, but also resistance to creep under compression. During PEMFC operation, applied compressive stress maintains intimate contact between the PEM and adjoining electrodes. Over time, the compressive stress in the PEM relaxes due to time-dependent viscoelastic material flow (creep). Creep and stress relaxation result in PEM thinning and loss of intimate contact with the electrodes, leading to gradual performance degradation. Severe PEM thinning eventually produces pinholes or micro-cracks, causing catastrophic failure of the PEMFC.

Membrane creep has been identified as one of the major physical degradation mechanisms for Nafion-based PEMs in low temperature (≤80 °C) applications.[14,16–19] At the higher operating temperatures of PBI membranes (120–200 °C), thermally activated creep may be more problematic. Past studies of PBI mechanical properties focused on stress-strain behavior of conventionally imbibed membranes.[20] Reports on sol-gel PBI membranes are limited to stress-strain behavior at ambient temperature.[9,21] Suvorov et al.[22] developed a computational methodology for modeling the stress relaxation of PBI-based MEAs, but that work offered little insight from the perspective of material development.

In conventionally imbibed PBI membranes, increasing acid doping level has a negative impact on mechanical properties.[20] One might expect inferior mechanical properties for sol-gel PBI membranes due to their much higher acid doping levels. In fact, the PPA process yields sol-gel membranes with acid doping levels as high as 40,[9,21] and with sufficient thermal and mechanical stability to enable their use in PEMFCs operated up to 200 °C. However, the long-term creep behavior of PBI membranes has not been previously explored.

From the point of view of structure-property relations, the creep resistance of a polymer network should increase with polymer volume fraction, molecular weight, chain rigidity, and physical cross-linking density.[23] As the polymer volume fraction (or solids content) increases, so do the number density of network strands and the elasticity of the gel network, at least in theory.[24] Considering that the polymer solids content can be as low as 5 wt % (or 3.8 vol %) in para-PBI sol-gel membranes, increasing the solids content may be the most obvious way to improve creep resistance. However, this approach is limited by PBI solubility in PPA, which sets an upper limit on solids content that can be obtained via the PPA process.

PBI solubility in PPA depends on monomer type (Fig. 1) and polymer molecular weight. In general, higher molecular weight and greater chain rigidity lead to lower solubility because of reduced entropy of mixing. On the other hand, monomers with greater polarity increase solubility due to favorable enthalpy of polymer-solvent interactions. Previous work[21,25–27] reports that the solubility of homopolymer PBI in PPA increases in the order 2OH-PBI < para-PBI < meta-PBI < 2,5-pyr-PBI < 3,5-pyr-PBI. The low solubility of 2OH-PBI has been ascribed to intermolecular hydrogen bonding and possible phosphate-mediated crosslinking,[21,26] which are absent in para-PBI. The greater chain flexibility of meta-PBI renders it more soluble than para-PBI.[28] Pyridine-based PBIs have even greater solubility due to the polar imine groups that promote favorable interaction with the PPA solvent.

Higher PBI solubility in PPA generally means higher solubility in PA, as well. Thus PBI solubility in PPA can increase polymer solids content, but this has a negative impact on gel thermal stability.[29] The thermal stability of PBI membranes corresponds inversely to solubility: 2OH-PBI > para-PBI > meta-PBI > 2,5-pyr-PBI > 3,5-pyr-PBI. The 2,5-pyr-PBI homopolymer can form a gel membrane at room temperature, but its stability at higher temperatures depends on the polymer solids content.[21] The 3,5-pyridine-PBI homopolymer is too soluble to form a PA-doped gel membrane, even at room temperature.[21]

With these facts in mind, this work reports the synthesis (via the PPA sol-gel process) and characterization of compressive creep in a series of sol-gel PBI membranes with increasing polymer solid content. To expand the polymer solids content range while achieving high temperature gel thermal stability, we have also synthesized high-solids copolymer PBIs by copolymerizing varying ratios of more- and less-soluble PBI monomers. The synthesis details and characterization of some of these copolymers have been reported previously.[27,30] The creep properties of a total of 23 membranes were evaluated by carrying out creep compression and creep recovery experiments. The creep behavior, especially recoverable compliance and extensional viscosity, are rationalized in terms of polymer solids content and PBI chemical structure.

EXPERIMENTAL

Chemicals

3,3′,4,4′-Tetraaminobiphenyl (TAB, polymer grade, ~97.5% purity) was donated by BASF Fuel Cells and used as received. 2,5-Dihydroxyterephthalic acid (2OH-TA, 98% purity, Aldrich) was purified by recrystallization in an ethanol and water mixture (EtOH:water = 3:2). Terephthalic acid and isophthalic acid (>99% purity, Amoco) were used as received. Pyridine dicarboxylic acids (2,5- and 3,5-PDAs, ~98% purity, Acros Chemical) were purified by recrystallization from dilute hydrochloric acid prior to use. PPA (115% conc.) was supplied by FMC Corporation and used as received.

Polymer Synthesis and Membrane Casting

The general preparation procedure of the PPA sol-gel PBI membrane follows that reported previously.[9] Diacid monomer(s) and TAB were added to a three-necked round-bottom flask equipped with an overhead mechanical stirrer, a water-cooled condenser, and nitrogen-purge inlet and outlet, followed by addition of PPA. The mixture was stirred and purged with nitrogen, and the reaction temperature was controlled by a programmable temperature controller with ramp and soak features. The typical final polymerization temperatures were approximately 190–220 °C. The polymerization time varied from 2 to 12 h, depending on the viscosity of the reaction mixture. During the polymerization, the reaction mixture became more viscous and developed a dark brown color.

The viscous polymerization solution was directly cast onto a glass plate using a Gardner film applicator with the gate thickness ranging from 5 to 25 mils. Hydrolyzing PPA to PA under controlled conditions led to membrane formation. Typically, exposing cast film to ambient air at 25 °C and relative humidity of 55% for 24 h converts all of the PPA to PA. Except for 3,5-pyridine-PBI homopolymer and some pyridine-based copolymers at certain comonomer ratios, PBI gel membranes were successfully formed.

PBI must have a molecular weight larger than a certain value to permit membrane formation. According to the literature,[31,32] the molecular weight should be above 11,000 Da, corresponding to an inherent viscosity (I.V.) of ~0.3 dL g^{-1}. The PBIs made by the sol-gel PPA process typically have high I.V. values, implying high molecular weights. In this study, the I.V. of the synthesized PBIs ranged from 0.66 to 5.04 dL g^{-1}. The I.V. values of the PBI products were measured using a Cannon Ubbelohde viscometer at 30 °C at a concentration of 0.2 g dry PBI per 100 mL concentrated sulfuric acid (96 wt %). The equation for calculating I.V. is given by $\ln(t/t_0)/C$, where C is the polymer concentration (0.2 g dL^{-1}), and t and t_0 are flow times of polymer solution and solvent, respectively.

Compression Creep and Creep Recovery Measurement

The compression creep and creep recovery method[33] was used to study the time-dependent creep behavior of the PBI gel membranes. The experiments were performed using a dynamic mechanical analyzer (TA Instruments, model RSAIII) using its built-in functionality for creep testing. In this work, a typical experiment consisted of a 20 h creep phase followed by a 3 h recovery phase. During the creep phase, a constant compressive force equivalent to a stress level of 0.1 MPa was applied to the membrane sample, followed by removal of this force at the start of recovery phase. The change of specimen thickness in response to the stress loading was recorded as a function of time during the entire experiment. Figure 2 shows the stress loading program for the experiment and the creep response of a viscoelastic material described by the Burgers model.[23] The creep response is expressed in terms of creep compliance, $J(t)$, defined as the ratio of time-dependent strain divided by applied compressive stress.

The geometry for the compression creep and creep recovery test setup as well as the definitions of stress and strain

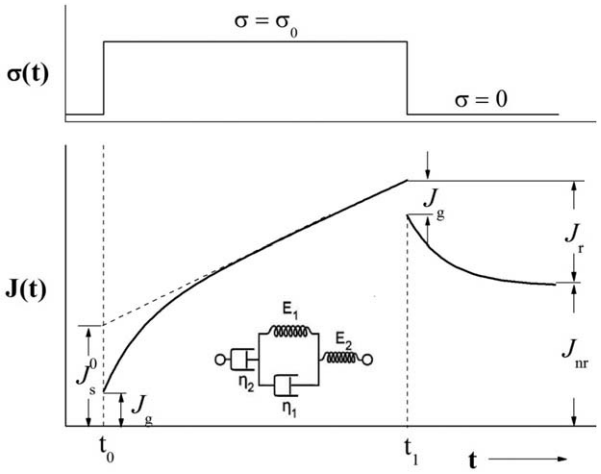

FIGURE 2 Creep and creep recovery of a Burgers material. The upper plot shows the stress loading history; the lower plot shows the creep compliance response of a viscoelastic material described by the Burgers model with indicated spring-and-dashpot representation.[23]

measures are illustrated in Figure S1 (Supporting Information). A parallel plate test fixture made of stainless steel was used. The plates were coated with a thin, dense layer of polytetrafluoroethylene (PTFE, $< 1\,\mu$m thick) to reduce the sliding friction between the specimen and the plate surfaces and thus approximate uniaxial compression. Data analysis assumed that the deformation was perfect uniaxial compression. For each membrane with distinct solids loading and monomer composition, the creep test was repeated 2–4 times using fresh specimens.

The test specimens were circular disks with diameter 6.0–6.5 mm and thickness 0.9–1.2 mm. All experiments were carried out at $180 \pm 0.5\,^{\circ}$C in a temperature-controlled oven with dry air circulation. The as-cast membranes contained 16–39% (w/w) of water at room temperature. At 180 °C, loss of water would cause substantial dimensional changes. To achieve dimensional stability, the test specimens were pre-conditioned at 180 °C for 24 h to drive off water. To prevent wrinkling of membranes during conditioning, the specimens were constrained between two smooth-surfaced PTFE blocks in a metal support frame. The PTFE blocks applied just enough force to ensure contact with the membrane without causing significant creep.

Membrane Composition

During the compression creep measurement, the specimen composition might change due to further loss of bound water, formation of oligomers of PPA, and exudation of PA. To track specimen composition changes during the test, two identical specimens were conditioned in the same environment. After conditioning, we characterized the composition of one specimen and used the other for the compression creep and creep recovery test. The composition of the latter was measured after creep testing. To determine the PA content, a sample was immersed in 40 mL DI water with stirring for several hours and then titrated with a sodium hydroxide solution of ~0.1 M to determine the equivalence point, from which the PA concentration can be calculated.[9] The polymer solids content was determined by dividing the absolute polymer weight (after titration and drying, free of PA and water) with the original sample weight (before titration). Typically, preconditioning reduced the water content in specimens to less than 2 wt %, with corresponding increase in polymer solids content. Polymer solids content typically increased during the creep test due to further elimination of water as well as exudation of PA.

RESULTS AND DISCUSSION

Description and Analysis of Creep Data

Creep compliance $J(t)$ under uniaxial compression (illustrated in Supporting Information Fig. S1) provides a direct measure of viscoelastic deformation under a constant compressive stress.[33] $J(t)$ is normally expressed as the engineering strain $\varepsilon(t)$ normalized with the nominal stress σ_0. However, considering that the gel membranes are soft and may undergo large deformations during testing, more appropriate measures are true strain $e(t)$ and true stress $s(t)$. Hence, our analysis uses $J(t)=e(t)/s(t)$ to define creep compliance. Supporting Information Figure S1 provides definitions of true strain and true stress. The compliance $J(t)$ measures the (normalized) amount of creep up to time t, and $\mathrm{d}J(t)/\mathrm{d}t$ indicates the creep rate. Low $J(t)$ and $\mathrm{d}J(t)/\mathrm{d}t$ correspond to high creep resistance.

Creep compliance data can be used to directly compare different membranes' creep deformation. Figure 3 shows the time-dependent creep behavior of four selected PBI membranes at 180 °C. These results introduce the main features associated with PBI membrane creep and its rationalization in terms of polymer solids content and polymer composition. For all membranes, the $J(t)$ curves in Figure 3 increase monotonically with time, $\mathrm{d}J(t)/\mathrm{d}t$ curves all decrease with time, and the positive curvature of $\mathrm{d}J(t)/\mathrm{d}t$ indicates deceleration of the creep rates.

We may arbitrarily choose values of $J(t)$ and $\mathrm{d}J(t)/\mathrm{d}t$ at the end of creep phase ($t = 20$ h) to assess the creep resistance of different materials. In Figure 3, the para-PBI membrane with $\phi = 10.8$ wt % has the highest values of $J_{20\mathrm{h}}$ and $\mathrm{d}J/\mathrm{d}t_{20\mathrm{h}}$, indicating that this material has inferior creep resistance compared to the other membranes. The para-PBI membrane with $\phi = 16.8$ wt % has lower $J_{20\mathrm{h}}$ and $\mathrm{d}J/\mathrm{d}t_{20\mathrm{h}}$ values: increasing the polymer solids content improves creep resistance. Changing the polymer chemistry from para- to meta-PBI (Fig. 1) and increasing ϕ to 19.8 wt % has mixed effects: $J_{20\mathrm{h}}$ increases slightly and $\mathrm{d}J/\mathrm{d}t_{20\mathrm{h}}$decreases but has higher curvature. The higher polymer solids content should improve creep resistance, but the more flexible meta-PBI chain structure has the opposite effect, decreasing creep resistance. The lowest $J_{20\mathrm{h}}$ and $\mathrm{d}J/\mathrm{d}t_{20\mathrm{h}}$values are observed for the meta-r-para-PBI copolymer membrane with the

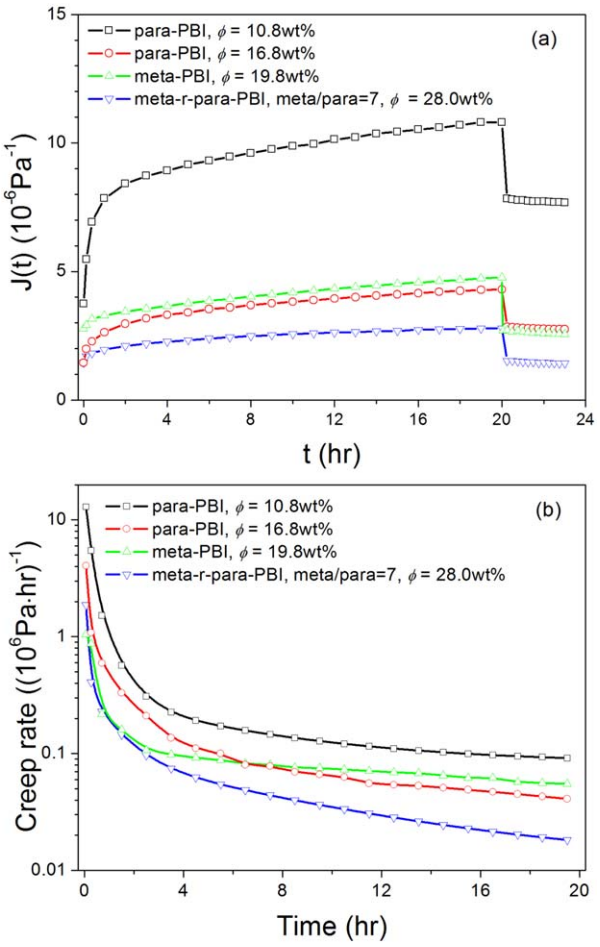

FIGURE 3 Time-dependent compression creep behavior of selected PBI membranes at 180 °C: (a) creep compliance $J(t)$ and (b) creep rate $dJ(t)/dt$. Indicated solids contents (ϕ) are values after creep testing. [Color figure can be viewed in the online issue, which is available at wileyonlinelibrary.com.]

highest solids content, $\phi = 28.0$ wt %. Clearly the increase in ϕ effectively reduces both creep compliance and creep rate.

Figure 3 illustrates the fact that solids content and copolymer composition play important roles in governing the membranes' creep resistance. However, choosing values of $J(t)$ and $dJ(t)/dt$ at an arbitrary time in the creep history introduces factors that may complicate data interpretation and rationalization. The curves in Figure 3 show that the creep compliances and rates vary markedly among these materials in the first 30 min of testing. Uncertainties in establishing the zero point of deformation (and thus strain) and composition variability, even among different specimens of the same material, affect the early stages of the creep history. Moreover, membrane composition continues to evolve throughout the creep test. For these reasons, single point values of $J(t)$ and $dJ(t)/dt$ may not be the best metrics for rationalizing creep behavior.

Instead, we propose a data analysis method that may be less sensitive to factors impacting creep history. The compliance curves in Figure 3(a) resemble the viscoelastic response predicted by the Burgers model (Fig. 2, inset), quantified by

$$J(t) = J_g + J_1(1 - e^{-t/\tau}) + t/\eta_0 \quad (1)$$

The compressive stress causes an instantaneous jump in compliance (J_g in Fig. 2) at time t_0 (which we may set as $t = 0$). Next, over an interval with characteristic time τ (one of two relaxation times in the Burgers model), $J(t)$ increases and $dJ(t)/dt$ decreases nonlinearly. At longer times, $dJ(t)/dt$ decreases sufficiently [Fig. 3(b)] so that $J(t)$ becomes nearly linear in t [Fig. 3(a)]. The nearly linear section of the $J(t)$ curve may be fit with the Maxwell model,[33]

$$J(t) = J_s^0 + t/\eta_0 \quad (2)$$

where J_s^0 and η_0 are the steady-state recoverable compliance and extensional viscosity, respectively. In the context of the Maxwell model, $(J_s^0)^{-1}$ characterizes the elastic energy stored in the material, η_0 characterizes the energy dissipated by viscous forces during steady-state creep, and the product $J_s^0\eta_0$ gives another characteristic relaxation time.[33] These parameters may vary with polymer solids content and chemical structure as well as process parameters such as temperature.

In this work, we attempt to rationalize the effects of polymer solids content and chemical structure on creep behavior using the Maxwell model, with linear regression of $J(t)$ data yielding two parameters, J_s^0 and η_0, for each data set. Although not reported here, nonlinear regression utilizing the Burgers model has also been explored. With four parameters available for regression, the quality of the Burgers model fit (eq 1) was judged to be reasonable, but not superior, to that of the Maxwell model (eq 2).

When the compressive stress is removed at the end of the creep period (t_1), viscoelastic gel membranes manifest an instantaneous compliance recovery [Fig. 3(a), sharp decrease in J at $t = 20$ h] followed by slower, approximately exponential compliance recovery. Data from this creep recovery phase can also be used to extract information on the elastic and viscous components of material behavior.

With regard to the details of data analysis, J_s^0 and η_0 can be determined by two methods.[33] In Method I, J_{ss}^0 and η_0 are extracted from the creep phase of the $J(t)$ curve by fitting its linear section with eq 2. The intercept of the fitted line with y-axis gives J_s^0 (as indicated in Fig. 2 at t_0), and the inverse of the slope (dt/dJ) gives η_0. In Method II, the creep recovery data are used to determine J_s^0 and η_0. First, the compliance recovery data are fit with an exponential decay function to determine J_{nr}, the "non-recoverable" or remnant compliance that cannot be recovered after the stress is removed. Then the recoverable compliance J_r equals $J(t_2) - J_{nr}$. By definition, J_r is equivalent to J_s^0.[33] Finally, η_0 is given by $(t_1 - t_0)/\left(J(t_1) - J_s^0\right)$, where J_s^0 is the value determined by Method I from the creep data. Method I and Method II produce the same results if the material perfectly obeys the Burgers or Maxwell models.

Although eq 2 provides a good approximation of the experimental $J(t)$ curve from $t = 4$ to 20 h, we observe a noticeable departure of the data from the Maxwell model. This must be true because the creep rate $dJ(t)/dt$ continues to decrease, albeit at a very slow rate [Fig. 3(b)]. This departure implies that the viscoelastic properties of the membranes are time-dependent. Polymer chains subjected to forces undergo rearrangement that causes in elasticity. Such microstructural changes are difficult to observe, and we did not attempt to quantify them in this work. In addition, membrane composition changes under the combined influences of mechanical load and temperature, as discussed below. Because the composition and structural variations have long time scales, compression creep tests may not attain steady-state creeping flow within a reasonable experimental time period. This may render Method I unreliable for estimating J_s^0;[33] Method II is then the preferred choice.

In this work, due to time restrictions, compression creep tests were run only for 20 h, followed by 3 h for creep recovery. Suspecting that steady state creeping flow may not have been attained, we evaluate J_s^0 and η_0 values based on two different periods during the creep test. The first period is between $t = 4$ and $t = 8$ h. We use Method I to determine J_s^0 and η_0 from the compliance data during this stage, denoted below as "short-time" results. Short-time J_s^0 and η_0 are more representative of the membranes' initial states, and, therefore, we associate them with membranes' initial polymer content, $\phi_{initial}$. The second period is the late creep stage between $t = 8$ h and $t = 20$ h. We use Method II to determine J_s^0 and η_0, denoted below as "long-time" results. Specifically, we determine J_s^0 from the creep recovery data, and η_0 from the compliance data between $t = 8$ and $t = 20$ h. Long-time J_s^0 and η_0 are representative of the final membrane state, and so we associate them with the membranes' final polymer solids content,ϕ_{final}. Comparing short-time results with long-time results may help rationalize the effect of changes in membrane composition. The main objective will be to rationalize the variations in J_s^0 and η_0 in terms of membrane's compositional and structural differences.

Effects of Conditioning on Membrane Composition and Creep

Conditioning or compressing membranes at elevated temperatures causes the membrane composition to change, which in turn changes the membranes' creep behavior. In this work, membrane composition was determined before pre-conditioning, after pre-conditioning, and after the creep and creep recovery test (Table 1). Increases in polymer solids content and reductions in PA/PBI ratios are observed after conditioning for all membranes. The primary cause is water loss caused by sample conditioning. As-cast PBI gel membranes are hygroscopic and consequently contain a substantial amount of water at room temperature. Free water molecules evaporate first as membranes are heated. At high enough temperatures, formation of oligomers of PPA also frees some bound water.

Increases in polymer solids content and reductions in PA/PBI ratios are also observed after compression creep. We attribute such changes mainly to loss of PA. When temperature is raised from 20 to 180 °C, the viscosity of PA decreases by one to two orders of magnitude. With enhanced fluidity and the aid of the compression force, PA can be exuded out of the membrane and lost in the open test environment. However, the reductions in PA/PBI ratios due to compression creep are much less pronounced that those due to conditioning, which reflects the ability of PBI membranes to retain PA even under compressive loads.

The effect of composition change on creep behavior can be inferred by comparing the short-time and the long-time creep properties. Figure 4 shows the comparison for para-PBI membranes; Supporting Information Figure S2 shows a similar set of plots for meta-PBI membranes. The points in Figure 4 and Supporting Information Figure S2 represent data derived from individual membrane specimens, including multiple runs for some samples with the same initial composition. Comparing the J_s^0 and η_0 values for various para-PBI membranes, clearly J_s^0 decreases and η_0 increases with increasing polymer solids content, for both short-time and long-time results (i.e., regardless of whether we consider $\phi_{initial}$ or ϕ_{final}). By decreasing the creep compliance and increasing the extensional viscosity, greater polymer solids content improves the creep resistance of para-PBI membranes, presumably due to the increase in macromolecular physical entanglements and interactions with ϕ. The increase of J_s^0 and decrease of η_0 with increasing ϕ are qualitatively the same trends as found for other viscoelastic polymer networks, both in experiment and theory.[23,24]

Comparing the short-time and long-time J_s^0 and η_0 values, as we move from short- to long-time results (from the left two plots to the right two plots in Fig. 4 and Supporting Information Fig. S2), the trend curve for J_s^0 shifts downward, and that for η_0 shifts upward. The shifts are more pronounced for membranes with lower polymer solids contents. These changes in J_s^0 and η_0 between short- and long-time scales must be related to the increase in PBI solids content over time during creep compression. On the other hand, the short-time and the long-time data cannot simply be superimposed; thus microstructural changes also contribute to the changes in creep properties. Finally, we notice that the long-time data have less scatter (higher R^2 values), suggesting that the creep compression reduces specimen-to-specimen heterogeneity. Similar trends are also apparent for the effect of composition change on the creep properties of meta-PBI membranes (Supporting Information Fig. S2).

Homopolymer PBI Membranes

Figure 5 compares the long-time creep properties of homopolymer PBI membranes (para-PBI, meta-PBI, 2,5-pyr-PBI, and 2OH-PBI), showing J_s^0 and η_0 as functions of ϕ_{final}. For the para-PBI and meta-PBI membranes, the variation of J_s^0 with ϕ_{final} follows an exponential decay. The J_s^0 values for para-PBI and meta-PBI membranes are clearly distinct, each

TABLE 1 Compositions of PBI Membranes Before Conditioning, After Conditioning, and After Compression Creep

		Before Pre-Conditioning			After Pre-Conditioning		After Compression Creep	
Sample Identity		Polymer (wt %, wet)	Polymer (wt %, dry)	PA/PBI Molar Ratio	Polymer (wt %)	PA/PBI Molar Ratio	Polymer (wt %)	PA/PBI Molar Ratio
Homopolymers								
2OH-PBI								
S-1		5.1	8.3	34.8	11.1	24.9	14.1	21.4
Para-PBI								
S-2		5.0	8.1	35.6	10.8	25.1	14.6	20.5
S-3		5.8	9.4	30.0	11.0	24.2	14.6	19.0
S-4		6.6	10.4	27.0	14.5	18.6	18.1	15.8
S-5		9.2	14.3	19.0	16.8	15.4	19.3	14.7
Meta-PBI								
S-6		8.4	11.3	24.8	19.6	12.9	24.6	10.7
S-7		15.7	22.8	10.6	24.5	9.7	31.1	7.9
S-8		15.7	21.3	11.6	25.6	9.1	31.9	7.6
S-9		16.5	19.8	12.8	28.3	9.0	35.6	7.4
S-10		20.7	29.3	7.6	33.6	6.8	43.1	5.2
2,5py-PBI								
S-11		15.2	22.5	10.9	25.9	9.2	31.8	7.3
Copolymers (A–B)	Composition (A:B ratio)							
Para-meta								
S-12	1:2.5	14.0	20.5	12.0	27.5	8.2	34.0	6.9
S-13	1:4	17.3	20.5	9.4	27.5	8.0	35.3	6.7
S-14	1:7	17.5	25.0	9.5	28.0	8.3	32.9	7.1
2,5py-meta								
S-18	3:1	15.2	21.4	11.6	28.8	7.7	31.3	7.3
S-19	1:9	18.9	26.4	8.8	35.0	6.0	39.8	5.3
2,5py-para								
S-16	3:1	13.7	20.2	12.5	30.1	7.1	32.8	6.8
S-17	4:1	15.9	22.1	11.1	30.2	7.3	37.6	6.1
3,5py-para								
S-21	1:5	14.9	21.0	11.8	26.0	9.6	31.4	7.7
S-22	1:1	17.1	23.0	10.5	38.7	5.2	44.9	4.4
S-23	3:1	19.5	24.8	9.5	36.3	5.6	44.3	4.5
2,5py-2OH								
S-15	3:1	15.2	22.5	10.9	30.2	7.3	32.7	6.8
3,5py-2OH								
S-20	1:1	14.6	21.8	11.3	26.4	9.4	31.3	8.5

following its own exponential correlation. The η_0 data for para-PBI and meta-PBI membranes both increase linearly with ϕ_{final}, with a better linear fit found for the para-PBI data.

Membranes made from para-PBI and meta-PBI prepared via the PPA sol-gel process have been studied previously.[9] Thermally stable para-PBI membranes can be prepared with as little as 5 wt % polymer (wet basis, Table 1), but relatively high J_s^0 values [Fig. 5(a)] indicate that such low-solids membranes are more susceptible to creep under compression. Increasing the para-PBI solids content reduces creep (J_s^0) and creep rate [i.e., increases η_0, Fig. 5(b)]. The trends of the curves through the para-PBI data suggest that even lower J_s^0 and higher η_0 values would result from further increases para-PBI solids content. However, the solubility limit for para-PBI in PPA prevents polymerization at higher

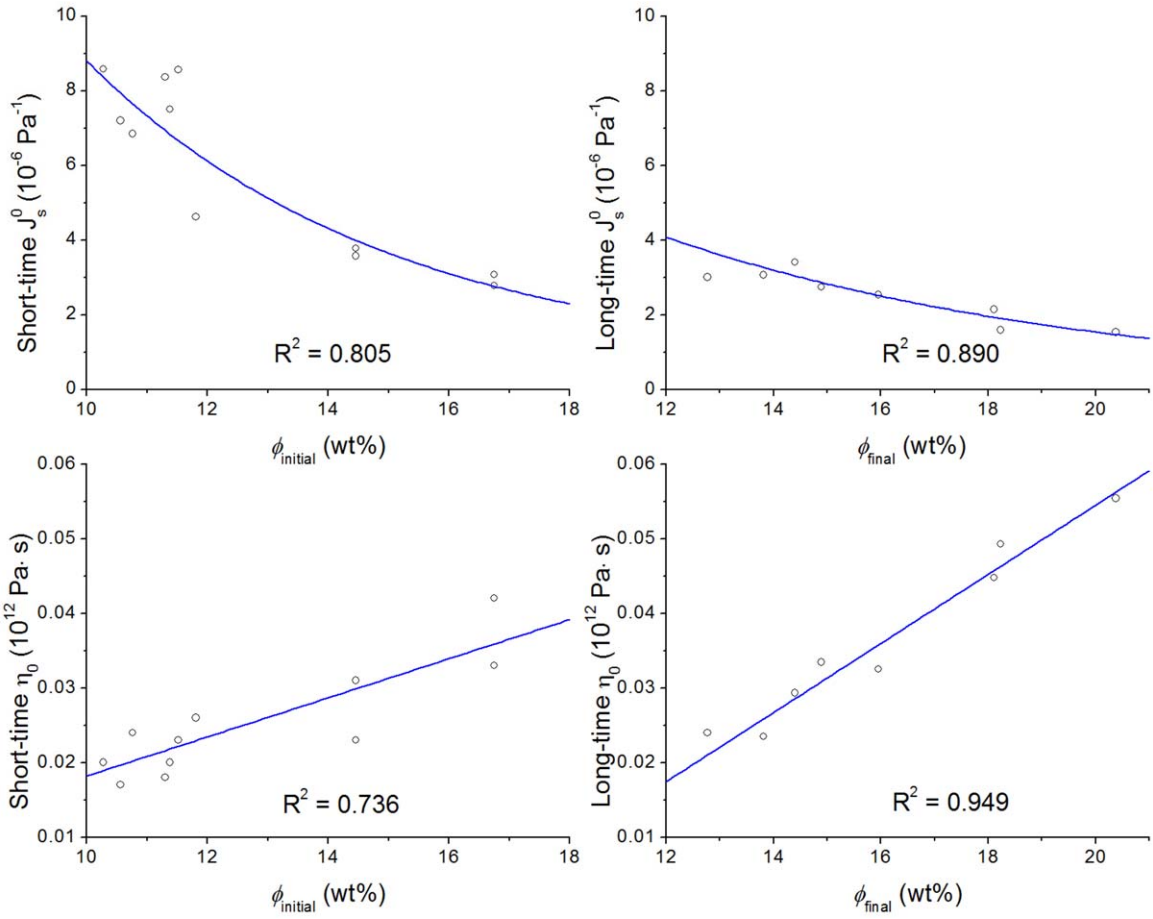

FIGURE 4 Comparison of the short-time and the long-time values (as defined in the text) of J_s^0 and η_0 for para-PBI membranes. The J_s^0 values were fit with exponential functions, and η_0 values were fit with lines. Coefficients of regression (R^2) are indicated; regression parameters are tabulated in Supporting Information. [Color figure can be viewed in the online issue, which is available at wileyonlinelibrary.com.]

concentrations and higher molecular weights, resulting in solutions that are too viscous to cast into films. The highest solids content that can be achieved in para-PBI membranes is about 9 wt % (as prepared, wet basis, Table 1, sample S-5), resulting in membranes with about 19–20% solids after the creep experiment (Fig. 5). At this limit, the polymerization time must be lowered before casting, which also lowers the polymer IV (IV = 1.1 dL g^{-1}, versus 5.1, 5.0, and 4.6 dL g^{-1} for samples S-2, S-3, and S-4, respectively).

Because meta-PBI has higher solubility in PPA,[13,27] membranes with higher polymer solids content can be prepared (Table 1). In particular, meta-PBI membranes with ϕ_{final} in the 30–45% range have lower J_s^0 and higher η_0 values than observed for para-PBI membranes (Fig. 5). However, comparing trend lines in Figure 5 shows that meta-PBI membranes would have higher creep and lower extensional viscosity than para-PBI membranes if the latter could be prepared at the same solids content.

For para-PBI, the p-phenylene linkage (Fig. 1) permits the polymer chain to assume a more extended conformation,[34,35] resulting in greater chain rigidity compared to meta-PBI. Hence, when stretched or bent, para-PBI molecules store more elastic energy. Moreover, the extended conformation in para-PBI may facilitate the formation of local ordered structures, as suggested by molecular dynamics simulations.[34–37] These locally ordered structures, formed due to hydrogen bonding[34,35] or other attractive chain–chain forces (such as van der Waals attraction),[36,37] could serve as physical crosslinks. These factors help rationalize the relative positions of the para-PBI and meta-PBI trend lines in Figure 5, as well as their creep behavior. The stiffer, more extended para-PBI forms strong gels at relatively low polymer solids content, but polymer solubility limits the maximum solids content that can be achieved. More flexible meta-PBI has greater solubility in PPA and thus can form membranes with higher solids content. However, meta-PBI's greater chain flexibility may result in gel networks with greater tendency to creep relative to the trend predicted for para-PBI.

The η_0 values for 2OH-PBI membranes [Fig. 5(b)] lie on the same trend line as those for para-PBI membranes. However, at the same solids content, 2OH-PBI membranes have much lower J_s^0 values and better creep resistance than para-PBI

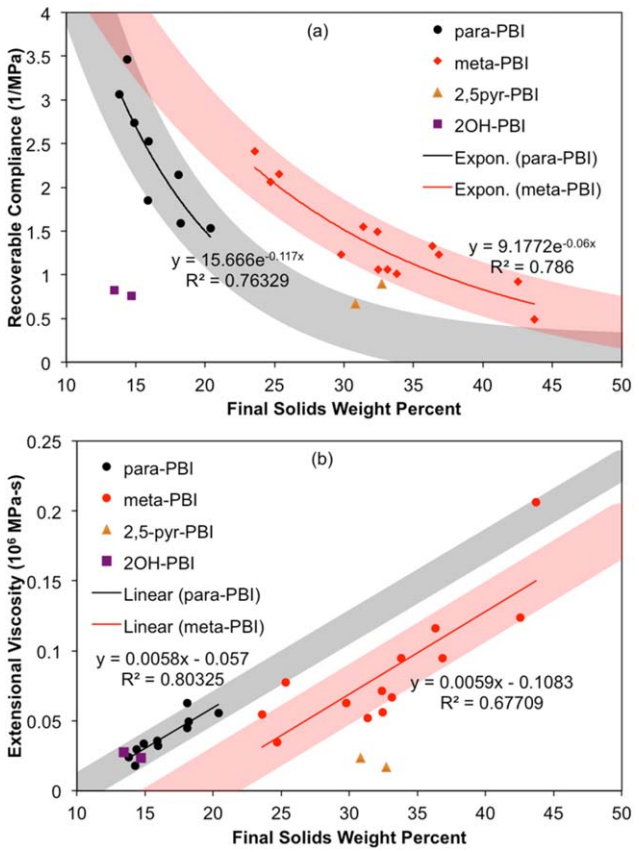

FIGURE 5 Steady-state recoverable compliance J_s^0 (a) and extensional viscosity η_0 (b) as functions of final solids wt % for para-PBI, meta-PBI, 2,5-pyr-PBI, and 2OH-PBI homopolymers. The solid curves are trend lines fit to the para-PBI and meta-PBI data. The shaded regions are extrapolations of the trend lines, broadened to visually encompass the data points. Each data point is a single compression creep experiment. [Color figure can be viewed in the online issue, which is available at wileyonlinelibrary.com.]

membranes [Fig. 5(a)]. The factors that contribute to the lower solubility of 2OH-PBI probably also explain its better creep resistance. In PA-imbibed 2OH-PBI, the —OH groups provide additional hydrogen bonding sites that increase the strength of chain–chain interactions and thus the networks' physical crosslinks.[34,35] FTIR spectra[25] have confirmed physical crosslinking in 2OH-PBI via phosphate linkages between 2OH-PBI hydroxyl groups and PA (or PPA). NMR spectra[26] indicate the presence of phosphate branches and possible crosslinking in 2OH-PBI that might impede chain slippage. These factors help rationalize the observations and explain why 2OH-PBI membranes with low polymer solids content have better creep resistance than para-PBI. The combination of high creep resistance and very good fuel cell performance[25] motivate our ongoing studies of homopolymer 2OH-PBI membranes.

The J_s^0 values for the 2,5-pyr-PBI membranes [Fig. 5(a)] lie below the trend curve for meta-PBI, indicating favorable elasticity in the 2,5-pyr-PBI gel network. However, the η_0 values for 2,5-pyr-PBI membranes [Fig. 5(b)] are quite low, especially considering the relatively high polymer solids content. In fact, 2,5-pyr-PBI membranes manifest high creep rates at 180 °C, making them less suitable than either meta- or para-PBI membranes. Based on our previous studies[21,27,30] of 2,5-pyr-PBI and 3,5-pyr-PBI homo- and copolymers, we believe that thermal stability limit for 2,5-pyr-PBI membranes may be just a few degrees higher than 180 °C. Polymer/solvent (2,5-pyr-PBI/PA) interactions may be favored relative to polymer/polymer attraction, resulting in a weaker network and thus higher creep rate.

Copolymer PBI Membranes

This section presents compression creep results for five random copolymer PBI systems, including 12 membranes of varying copolymer ratios, as listed in Table 1. The rationalization of compression creep data in terms of polymer structure is complicated because there are now two compositional variables, total polymer solids content (ϕ) and copolymer ratio. Combining different PBI copolymer repeat units in a random copolymer will change chain rigidity, chain–chain interactions, and chain-solvent interactions, all of which affect polymer solubility, solids content, and the strength of physical crosslinks.

In practice, low polymer solubility limits the polymer solids content that can be achieved in 2OH-PBI and para-PBI membranes. This precludes the synthesis of high-solids, low creep membranes based on the relatively rigid 2OH-PBI and para-PBI homopolymer structures. To overcome this limitation, we have explored copolymers that combine more soluble polymer repeat units (meta-PBI, 2,5-py-PBI, or 3,5-py-PBI; see Fig. 1) with less soluble polymer repeat units (para-PBI, 2OH-PBI).[27,30] We envision two routes to membranes with low creep compliance. First, beginning with the more soluble meta-PBI repeat unit, co-polymerizing with a less soluble repeat unit (like para-PBI) may produce stiffer, more rigid copolymers while achieving high solids content. Referring to Figure 5(a), this represents moving downward (toward lower compliance) from the meta-PBI curve at fixed ϕ_{final}. The second route begins with less-soluble para-PBI (or 2OH-PBI) repeat unit and co-polymerizing with more soluble repeat units to produce copolymers with higher solids content and lower creep compliance. Again referring to Figure 5(a), this could be viewed as moving down the para-PBI trend curve.

Meta-Based Copolymers

Figure 6 shows values for steady-state recoverable compliance, J_s^0, for copolymers containing primarily the meta-PBI repeat unit. The three para-meta copolymers contain primarily meta-PBI repeat units with minority fractions of the less-soluble para-PBI repeat unit (molar ratios 1:7, 1:4, and 1:2.5, corresponding to 12.5%, 20%, and 29% para-PBI). All three of the para-meta copolymers have J_s^0 values similar to those found for meta-PBI homopolymer at about the same final solids wt %. The extensional viscosity results (Supporting Information Fig. S3) are similar: the η_0 values for all three

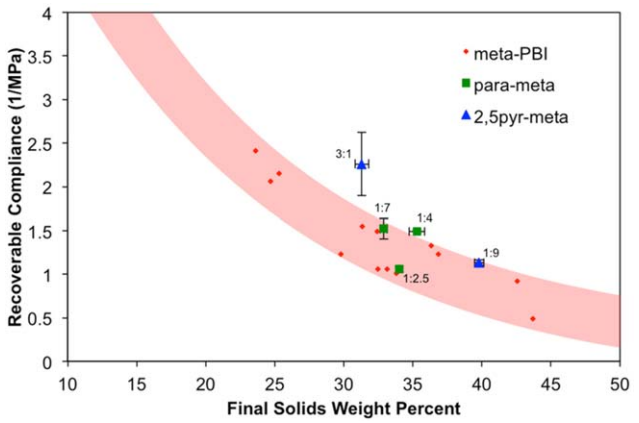

FIGURE 6 Steady-state recoverable compliance as a function of final solids wt% for meta-PBI homopolymer and meta-based copolymers. For the copolymers, each data point is an average of 2–4 replicate measurements for copolymers with the same copolymer ratio (as indicated in the plot). The shaded region is the extrapolated trend curve for meta-PBI homopolymer from Figure 5(a). [Color figure can be viewed in the online issue, which is available at wileyonlinelibrary.com.]

para-meta copolymers are the same as those for meta-PBI homopolymer at the same final solids wt %. Thus the addition of minority amounts of less-soluble para-PBI repeat units does not have the anticipated stiffening effect. The creep resistance of these para-meta copolymers is dominated by the majority meta-PBI component.

We also synthesized and tested copolymers of meta-PBI with the more-soluble 2,5-pyr-PBI repeat unit. For the copolymer containing 10 mol % 2,5-pyr repeat unit (ratio 1:9), the membranes' average J_s^0 value (Fig. 6) and η_0 value (Supporting Information Fig. S3) are also similar to those for meta-PBI homopolymer. Again, the majority meta-PBI repeat unit dominates the properties of this copolymer, as found for the para-meta copolymers. For the copolymer containing 75 mol % 2,5-pyr repeat unit (ratio 3:1), the average J_s^0 value (Fig. 6) is significantly larger than that found for meta-PBI homopolymers. The polarity of imine nitrogen in the 2,5-pyr repeat unit creates an energetically favorable interaction with the PA solvent, leading to increased polymer solubility. The favorable chain-solvent interactions result in weakening of the chain–chain attraction. We believe that this reduces the strength of physical crosslinks in this material, resulting in reduction of the membranes' creep resistance, as indicated by the higher J_s^0 values.

Para-Based Copolymers

Figure 7 shows J_s^0 values for copolymers containing primarily para-PBI repeat units. The 2,5-pyr-para copolymers (2:1 and 3:1 ratios) and two of the 3,5 pyr-para copolymers (1:1 and 3:1 ratios) have J_s^0 values that lie significantly above the extrapolated trend curve for para-PBI homopolymer (shaded region). All of these copolymers contain at least 50% of the more-soluble 2,5-pyr or 3,5-pyr repeat units, and 50% or less of the para repeat unit. The presence of a majority of the 2,5-pyr or 3,5-pyr repeat unit makes these copolymers more soluble, enabling the production of membranes with higher solids wt% than can be achieved for para-PBI homopolymer. This can be ascribed to the more energetically favorable polymer-solvent interactions. However, the chain–chain interactions in these copolymers are weaker than in para-PBI homopolymers. This results in weaker physical crosslinks in the copolymer gel networks, manifested in the higher J_s^0 valuesthan might be expected for para-PBI homopolymers.

The steady-state recoverable compliance for 3,5pyr-para copolymer (1:5 ratio) is remarkable (Fig. 7). This copolymer is 83% para-PBI repeat unit with only 17% of the highly soluble 3,5-pyr repeat unit. This copolymer has sufficient solubility in PPA to enable production of a membrane containing almost 15% solids before pre-conditioning, with a final post-creep solids content of 31.4 wt % (Table 1). The average J_s^0 value for this copolymer lies on the extrapolated trend curve for para-PBI homopolymer. The predominant para-PBI repeat unit probably promotes the formation of relatively strong physical crosslinks in the final PA-imbibed membrane, resulting in the low compliance. Thus copolymerizing a small fraction of highly soluble repeat unit with a majority of less soluble repeat unit (like para-PBI or 2OH-PBI) gives us a promising route to stiff, low compliance membranes.

Figure 7 also shows J_s^0 values for 2OH-PBI homopolymer and related copolymers, which display similar trends to those of para-based copolymers. The average J_s^0 value for the 2,5-pyr-2OH copolymer (3:1 ratio) is essentially the same as that for 2,5-pyr-para copolymer with 3:1 monomer ratio. The presence of a minority amount of the less-soluble repeat unit

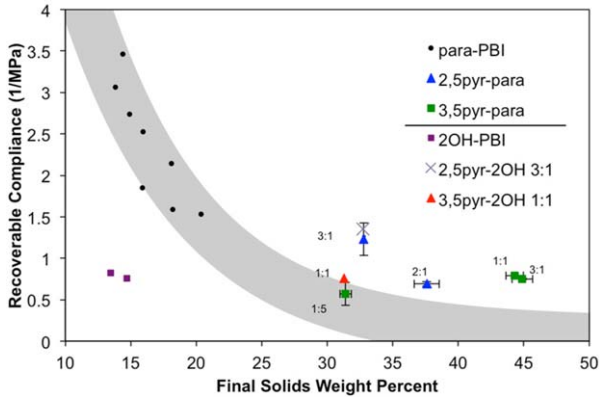

FIGURE 7 Steady-state recoverable compliance as a function of final solids wt % for para-PBI and 2OH-PBI homopolymers and related copolymers. For the para-based copolymers, each data point is an average of 2–4 replicate measurements for copolymers with the same copolymer ratio (as indicated in the plot). The data points for the homopolymers and the 2OH-based copolymers are single measurements. The shaded region is the extrapolated trend curve for para-PBI homopolymer from Figure 5(a). [Color figure can be viewed in the online issue, which is available at wileyonlinelibrary.com.]

(2OH or para) has little impact on compliance. Both copolymers contain 75 mol % of the more soluble 2,5-pyr repeat unit, giving them more favorable polymer-solvent interactions, possibly at the expense of producing weaker polymer–polymer interactions. If this is the case, then inclusion of high fractions of the more-soluble 2,5-pyr monomer leads to weaker physical crosslinks and thus more compliant gel networks.

The average J_s^0 value for the 3,5-pyr-2OH copolymer (1:1 ratio) about the same as that of the 2OH-PBI homopolymer. Copolymerizing equal amounts of 3,5-pyr and 2OH repeat units results in a copolymer that is more soluble than 2OH-PBI homopolymer. Consequently we can prepare 3,5-pyr-2OH copolymer membranes with higher solids wt %, which should improve creep resistance. However, for reasons given above, the more soluble copolymer must also have weaker physical crosslinks, which reduces network strength and creep resistance. The average J_s^0 value for the 3,5-pyr-2OH copolymer reflects this compromise. We are investigating 3,5-pyr-2OH copolymers with ratios less than 1:1 in an attempt to prepare membranes with higher solids wt% and lower J_s^0 values than the 2OH-PBI homopolymer.

Results for the extensional viscosities of membranes composed of para-based and 2OH-based copolymers (Supporting Information Fig. S4) are generally consistent with the trends for J_s^0. With the exception of the 3:1 ratio 2,5-pyr-para copolymer membrane, all of the η_0 values for para-based copolymer membranes lie below the extrapolated η_0 trend line for para-PBI homopolymer. This observation is consistent with the view that these copolymers have weaker physical crosslinks and thus are more susceptible to continuous deformation under compressive stress. The η_0 values for 2,5-pyr-para and 2,5-pyr-2OH copolymer membranes, both 3:1 ratio, are greater than predicted for para-PBI homopolymer. However, the statistical significance of these comparisons have not been established. Of course, the extrapolation of the η_0 trend line for para-PBI homopolymer may be questionable, as well.

DISCUSSION AND CONCLUSIONS

Proton exchange membranes based on PBI polymers have emerged as viable alternatives to Nafion® for use in fuel cells and other applications. Because PBI membranes utilize PA as the electrolyte, they can operate at high temperatures (120–200 °C) without the need for careful humidity control. The recent development of the PPA process offers a simple, convenient method to synthesize stable sol-gel membranes with high PA:PBI polymer repeat unit ratios. PBI membranes made by the PPA process have been operated for extended time periods in PEMFCs at elevated temperatures. However, the low solids content and elevated temperatures make these membranes susceptible to creep when subjected to compression in fuel cell stacks.

To improve the creep resistance of PBI membranes made by the PPA sol-gel process, we initially hypothesized that increasing the polymer solids content would lead to stronger sol-gel networks with lower creep. To this end, we synthesized and characterized 23 different PBI polymers, and carried out over 60 distinct, 24 h creep tests, to investigate the effects of polymer solids content and chemical composition on PBI creep behavior. In this study, we were careful to precondition our samples and keep track of composition changes due to loss of water and PA. To our best knowledge, the current work is the first experimental report on the compression creep behavior of PA-doped PBI sol-gel membranes at relevant operating temperatures for high-temperature PEMFCs.

Beginning with the "benchmark" para-PBI homopolymer, we investigated the effects of pre-conditioning and compression on membrane composition. Both pre-conditioning and prolonged compression result in significant increases in polymer solids content, along with corresponding changes in the membranes' viscoelastic properties. Increasing polymer solids content was accompanied by decreasing J_s^0 and increasing η_0, which may be rationalized in terms of increasing gel network junction density.[23] The results confirm that the creep resistance of PBI membranes improve with increasing polymer solids content. However, the solubility of para-PBI in PPA limits the solids content that can be achieved in membranes made from para-PBI homopolymer.

The structure of the meta-PBI polymer leads to polymer chains with greater flexibility and higher solubility in PA. Consequently, one can prepare meta-PBI membranes with considerably higher solids content. As found for para-PBI, the creep resistance of meta-PBI membranes shows distinct improvement as the polymer solids content increases. However, meta-PBI membranes have significantly higher values of recoverable compliance, and lower extensional viscosity values, than one might expect for para-PBI, at least based on extrapolation of the para-PBI trend curves to higher solids content. The greater solubility of meta-PBI enables production of higher solids membranes, but the greater chain flexibility reduces network strength. Ultimately, we found that meta-PBI membranes could be prepared with J_s^0 values significantly lower than those of para-PBI membranes, but the solids contents of the former are at least twice as high as the latter.

Low-solids 2OH-PBI homopolymer membranes also had quite low J_s^0 values. However, the very low solubility of 2OH-PBI in PPA limited our ability to synthesize higher solids 2OH-PBI membranes with even smaller J_s^0 values and thus better creep resistance.

The challenge lies in finding an optimal compromise between factors that increase polymer solubility in PPA, and those that increase sol-gel network strength in PA. The factors that tend to increase polymer solubility (i.e., use of monomers that produce more flexible polymer chains or promote polymer-solvent interactions) also tend to decrease sol-gel network strength. PBI copolymers offer us a way to explore this tradeoff in ways that are not possible with homopolymers.

To this end, we synthesized and characterized a variety of random copolymers incorporating two PBI polymer repeat units with differing solubilities in PPA. We found that copolymerizing a small amount of highly soluble repeat unit (e.g., 2,5-pyr or 3,5-pyr) with a dominant fraction of low-solubility repeat unit (e.g., para-PBI or 2OH-PBI) leads to membranes with a promising combination of low to moderate solids content and low creep compliance. Such copolymers may offer a good compromise between solubility in PPA (yielding higher solids content and thus higher density of gel network junctions) and stronger polymer–polymer interactions in PA (favoring gel thermal stability and network mechanical strength). We are continuing to explore this part of the composition parameter space to identify optimal compositions that yield superior electrochemical performance as well as creep resistance. Overall, this work demonstrates the feasibility of improving the creep properties of PBI gel membranes by rational design of membrane composition and PBI structure.

ACKNOWLEDGMENT

The authors would like to thank BASF SE for financial support of this work.

REFERENCES AND NOTES

1 J. S. Wainright, J.-T. Wang, D. Weng, R. F. Savinell, M. Litt, *J. Electrochem. Soc.* **1995**, *142*, L121–L123.

2 J. T. Wang, J. Wainright, H. Yu, M. Litt, R. F. Savinell, *Proc. Electrochem. Soc.* **1995**, *95-23*, 202–213.

3 S. R. Samms, S. Wasmus, R. F. Savinell, *J. Electrochem. Soc.* **1996**, *143*, 1225–1231.

4 J.-T. Wang, J. S. Wainright, R. F. Savinell, M. Litt, *J. Appl. Electrochem.* **1996**, *26*, 751–756.

5 R. Bouchet, E. Siebert, *Solid State Ionics* **1999**, *118*, 289–299.

6 B. Xin, O. Savadogo, *J. New Mater. Electrochem. Syst.* **1999**, *2*, 95–101.

7 C. Hasiotis, Q. Li, V. Deimede, J. K. Kallitsis, C. G. Kontoyannis, N. J. Bjerrum, *J. Electrochem. Soc.* **2001**, *148*, A513–A519.

8 H.-J. Kim, S. J. An, J.-Y. Kim, J. K. Moon, S. Y. Cho, Y. C. Eun, H.-K. Yoon, Y. Park, H.-J. Kweon, E.-M. Shin, *Macromol. Rapid Commun.* **2004**, *25*, 1410–1413.

9 L. Xiao, H. Zhang, E. Scanlon, L. S. Ramanathan, E.-W. Choe, D. Rogers, T. Apple, B. C. Benicewiz, *Chem. Mater.* **2005**, *17*, 5328–5333.

10 P. J. Flory, *Faraday Discuss. Chem. Soc.* **1974**, *57*, 7–18.

11 M. Molleo, T. J. Schmidt, B. C. Benicewicz, In *Encyclopedia of Sustainability Science and Technology*; R. A. Meyers, Ed.; Springer-Verlag: New York, **2012**; pp 391–431.

12 D. C. Seel, B. C. Benicewicz, L. Xiao, T. J. Schmidt, In *Handbook of Fuel Cells: Advances in Electrocatalysis, Materials, Diagnostics and Durability*; W. Vielstich, H. A. Gasteiger, H. Yokikawa, Eds.; Wiley: Chichester, UK, **2009**; Vols. *5–6*, Chapter 19, pp 300–312.

13 J. Mader, L. Xiao, T. Schmidt, B. C. Benicewicz, *Adv. Polym. Sci.* **2008**, *216*, 63–124.

14 R. Borup, J. Meyers, B. Pivovar, Y. S. Kim, R. Mukundan, N. Garland, D. Myers, M. Wilson, F. Garzon, D. Wood, P. Zelenay, K. More, K. Stroh, T. Zawodzinski, J. Boncella, J. E. McGrath, M. Inaba, K. Miyatake, M. Hori, K. Ota, Z. Ogumi, S. Miyata, A. Nishikata, Z. Siroma, Y. Uchimoto, K. Yasuda, K.-I. Kimijima, N. Iwashita, *Chem. Rev.* **2007**, *107*, 3904–3951.

15 U.S. Dept. Energy, An Integrated Strategic Plan for the Research, Development, and Demonstration of Hydrogen and Fuel Cell Technologies; **2011**. Available at: http://www1.eere.energy.gov/hydrogenandfuelcells/pdfs/program_plan2011.pdf, accessed on April 30, 2015.

16 F. Bauer, S. Denneler, M. Willert-Porada, *J. Polym. Sci. Part B: Polym. Phys.* **2005**, *43*, 786–795.

17 K. A. Patankar, D. A. Dillard, S. W. Case, M. W. Ellis, Y.-H. Lai, C. S. Gittleman, *Fuel Cells* **2012**, *5*, 787–799.

18 Y. Li, D. A. Dillard, S. W. Case, M. W. Ellis, Y.-H. Lai, C. S. Gittleman, D. P. Miller, *J. Power Sources* **2009**, *194*, 873–879.

19 P. W. Majsztrik, A. B. Bocarsly, J. B. Benziger, *Macromolecules* **2008**, *41*, 9849–9862.

20 Q. Li, J. O. Jensen, R. F. Savinell, N. J. Bjerrum, *Prog. Polym. Sci.* **2009**, *34*, 449–477.

21 L. Xiao, H. Zhang, T. Jana, E. Scanlon, R. Chen, E.-W. Choe, L. S. Ramanathan, S. Yu, B. C. Benicewicz, *Fuel Cells* **2005**, *5*, 287–295.

22 A. P. Suvorov, J. Elter, R. Staudt, R. Hamm, G. J. Tudryn, L. Schadler, G. Eisman, *Int. J. Solids Struct.* **2008**, *45*, 5987–6000.

23 W. W. Graessley, *Polymer Liquids and Networks: Structure and Properties*; Taylor & Francis: New York, **2004**.

24 M. Rubinstein, R. H. Colby, *Polymer Physics*; Oxford University Press: New York, **2003**.

25 S. Yu, B. C. Benicewicz, *Macromolecules* **2009**, *42*, 8640–8648.

26 S. Suarez, N. K. A. Kodiweera, P. Stallworth, S. Yu, S. G. Greenbaun, B. C. Benicewicz, *J. Phys. Chem. B* **2012**, *116*, 12545–12551.

27 M. Molleo, X. Chen, H. J. Ploehn, B. C. Benicewicz, *Fuel Cells* **2014**, *14*, 16–25.

28 S. Yu, H. Zhang, L. Xiao, E.-W. Choe, B. C. Benicewicz, *Fuel Cells* **2009**, *9*, 318–324.

29 P. E. Cassidy, *Thermally Stable Polymers*; Marcel Dekker: New York, **1980**.

30 M. Molleo, X. Chen, H. J. Ploehn, B. C. Benicewicz, *Fuel Cells* **2015**, *15*, 150–159.

31 R. He, Q. Li, A. Bach, J. O. Jensen, N. J. Bjerrum, *J. Membr. Sci.* **2006**, *277*, 38–45.

32 J. S. Wainright, M. H. Litt, R. F. Savinell, In *Handbook of Fuel Cells: Fundamentals, Technology and Applications*; Wiley: New York, **2003**; pp 436–446.

33 J. D. Ferry, *Viscoelastic Properties of Polymers*, 3rd ed.; Wiley: New York, **1980**; pp 35–129.

34 S. Li, J. R. Fried, J. Colebrook, J. Burkhardt, *Polymer* **2010**, *51*, 5640–5648.

35 S. Zhu, L. Yan, D. Zhang, Q. Feng, *Polymer* **2011**, *52*, 881–892.

36 V. Padmanabhan, S. K. Kumar, A. Yethiraj, *J. Chem. Phys.* **2008**, *128*, 124908.

37 V. Padmanabhan, S. K. Kumar, *J. Chem. Phys.* **2011**, *134*, 174902.